In conclusion, we wish to suggest that we may have succeeded in unravelling the contributions of the cavity term and the dipolar solute/solvent interaction term to the free energy of solution by the procedure of restricting consideration to the nonprotonic aliphatic *select solvents*.[8] Others taking a similar approach may have failed because they encountered complications of hydrogen bonding by protonic solvents, and variable solute dipole/solvent induced dipole (polarizability) effects in the case of aromatic solvents. However, Abraham and Reisse[35] have succeeded in subtracting out the cavity term contributions to a number of processes in hydroxylic solvents by direct calculation.

We also wish to point out that many earlier correlations (generally of poor precision) with the Hildebrand solubility parameter have been for properties which include important dipolar solute/solvent interaction effects. We suggest that such properties are likely to be much better correlated by the π^* parameter, by dual solvent parameter equations in π^* and δ_H, or, where solute/solvent hydrogen bonding effects also apply, by equations involving linear combinations of π^*, δ_H, α, and β, as appropriate (α and β being measures of solvent hydrogen bond donor acidity and hydrogen bond acceptor basicity).[3] Thus, we have recently demonstrated[36] that solvent effects on some fluorescence probes, which had been related to solvent δ_H values by Coosemans and co-workers[37] and by Reeves and co-workers,[38] were much better correlated by multiple linear regression equations in π^*, α, and β.

We are grateful to a referee for pointing out that Krishnan and Friedman[39] have calculated enthalpies of solution of gaseous nondipolar solutes by using an equation that contains an electrostatic term in μ and a term derived from solubility parameter theory; compare our two-term equation in π^* (also proportional to μ in the case of the select solvents)[8] and δ_H. We acknowledge that this earlier approach of Krishnan and Friedman is conceptually not dissimilar to ours. Unfortunately, it is not possible to make any direct comparison between the two methods because Krishnan and Friedman dealt with enthalpies of solution, whereas in the present work it is the free energy of solution that is the relevant thermodynamic parameter. It does deserve comment, however, that the earlier workers had suggested that solute/solvent electrostatic interaction terms account for ca. 15–30% of the ΔH_s° values for *n*-hexane solute in dipolar solvents, whereas our analysis indicates that the contributions of solute/solvent interactions to ΔG_s° values of the alkanes are essentially nil.

Acknowledgment. The work by R.W.T. was supported in part by a grant from the Public Health Service. The work by M.J.K. was done under Naval Surface Weapons Center Independent Research Task IR-210.

(35) Abraham, M. H.; Nasehzadeh, A.; Moura Ramos, S. S.; Reisse, J. *J. Chem. Soc., Perkin Trans. 2* **1980**, 854.
(36) Kamlet, M. J.; Dickinson, C.; Taft, R. W. *Chem. Phys. Lett.* **1981**, *77*, 69.
(37) Coosemans, L.; de Schryver, F. C.; van Dormael, A. *Chem. Phys. Lett.* **1979**, *65*, 95.
(38) Reeves, R. L.; Maggio, M. S.; Costa, L. F. *J. Am. Chem. Soc.* **1974**, *96*, 5917.
(39) Krishnan, C. V.; Friedman, H. L. *J. Phys. Chem.* **1971**, *75*, 3598.

Electronic Structure of Free-Base and Transition-Metal Tetraazaporphyrins

Ziva Berkovitch-Yellin† and D. E. Ellis*

Contribution from the Department of Chemistry and Materials Research Center, Northwestern University, Evanston, Illinois 60201. *Received December 15, 1980*

Abstract: Electronic energy levels and charge distribution for metal-free tetraazaporphyrin (H_2TAP) and transition-metal tetraazaporphyrins (MTAP, M = Fe and Cu) have been calculated in the one-electron Hartree–Fock–Slater model. Spin densities were obtained for CuTAP and FeTAP. Optical transitions, photoelectron binding energies, and hyperfine fields are presented for comparison with available data and previous theoretical works. Density difference contour maps and a Mulliken atomic orbital population analysis are used to discuss similarities to the related porphine systems. Most bonding features expected on the basis of semiempirical calculations and chemical intuitive arguments are observed in the electron density maps. A transition-state procedure was used to investigate several optical transitions as well as one-electron binding energies. Spectroscopic features are in fair agreement with experiment and with extended-Hückel model results of Gouterman et al.

A variety of metallophthalocyanines (MPc) exist, consisting of essentially planar molecules of D_{4h} symmetry having the central metal ion coordinated to four nitrogen ligands. MPc's differ from the chemically similar porphyrins in replacing four carbon atoms of the porphin ring by nitrogen. The substitution of N (and other species) on the carbon skeleton modifies the interaction between the metal ion d electron and valence-electron states of the ring to a significant degree. One goal of the present work is to begin a systematic study of these metal d/ring interactions. These studies have some relevance to experimental interest in one-dimensional conducting stacks of MPc's, as found in "molecular metals" like $NiPcI_x$.[1]

The phthalocyanines are valuable as commercial pigments, due to intense absorption bands in the visible region. Theoretical models based upon semiempirical calculations have been able to explain most features of the optical spectra, but require the use of adjustable parameters.[2-5] Recently, good quality gas-phase photoelectron spectra for a number of Pc's have become available.[6]

† Department of Structural Chemistry, Weizmann Institute, Rehovoth, Israel.

(1) J. L. Petersen, C. J. Schramm, D. R. Stojakovic, B. M. Hoffman, and T. J. Marks, *J. Am. Chem. Soc.*, **99**, 288 (1977); C. J. Schramm, D. R. Stojakovic, B. M. Hoffman, and T. J. Marks, *Science*, **200**, 47 (1978).
(2) A. M. Schaffer and M. Gouterman, *Theor. Chim. Acta*, **25**, 62 (1972); previous Hückel calculations in D_{4h} symmetry include: S. Basu, *Indian J. Phys.*, **28**, 511 (1954), and M. Gouterman, G. H. Wagniere, and L. L. Snyder, *J. Mol. Spectrosc.*, **11**, 103 (1963).
(3) A. Henriksson and M. Sundbom, *Theor. Chim. Acta*, **27**, 213 (1972).
(4) A Henriksson, B. Roos, and M. Sundbom, *Theor. Chim. Acta*, **27**, 303 (1972).
(5) I. Chen and M. Abkowitz, *J. Chem. Phys.*, **50**, 2237 (1969); I. Chen, *J. Mol. Spectrosc.*, **23**, 131 (1967).
(6) J. Berkowitz, *J. Chem. Phys.*, **70**, 2819 (1979). Thin film data were obtained by M. V. Zeller and R. G. Hayes, *J. Am. Chem. Soc.*, **95**, 3855 (1973); D. N. Hendricksen, J. M. Hollander, and W. L. Jolly, *Inorg. Chem.*, **8**, 2642 (1969); E. E. Koch and W. D. Grobman, *J. Chem. Phys.*, **67**, 837 (1977).

0002-7863/81/1503-6066$01.25/0

Table I. Atomic Coordinates (in Bohrs) for H_2TAP and MTAP Calculations

	H_2TAP (shared H)		H_2TAP (bonded H)		CuTAP[a]		FeTAP[a]	
atom	x	y	x	y	x	y	x	y
N	6.4651	0.0	3.8770	0.0	3.6553	0.0	3.6403	0.0
C	2.3417	5.2921	2.0865	5.3986	2.0780	5.1855	2.0977	5.1831
N′	2.7411	2.7411	4.5722	4.5722	4.4901	4.4901	4.4997	4.4997
C′	4.7590	6.5510	1.2673	7.9985	1.3219	7.8250	1.3147	7.8074
H	4.8970	8.4142	2.4874	9.4138	2.5900	9.4511	2.5247	9.4014
H_1	2.7411	0.0	2.2915	0.0				
H_2	−2.7411	0.0	−2.2915	0.0				

[a] Metal at $x = y = 0$.

Finally, the sensitivity of modern X-ray and neutron techniques makes it probable that reliable experimental charge and spin density maps for these systems will appear in the near future.[7] Thus we have undertaken a comprehensive study of energy levels and electron densities, using a first-principles local density model without adjustable parameters, on the simpler related tetraazaporphyrin ring (TAP).

Theory and Computational Procedure

We use the spin-unrestricted one-electron local density (LD) model to obtain self-consistent wave functions and energies for the molecule.[8-10] A fixed choice of electron configuration (orbital occupation numbers) can be made, or else Fermi–Dirac statistics are imposed to determine the charge and spin densities. The Hamiltonian for states of given spin σ, h_σ, is taken to be a simple functional of the densities, usually within the statistical exchange approximation.[8] The basic theory is available in the literature; it is generally understood that providing sufficient care is taken with numerical approximations, results are of about "Hartree–Fock" (HF) quality for a variety of properties. The computational effort required for molecules like metalloporphyrins is at least one order of magnitude less for local density calculations as compared to HF calculations with modest basis sizes.

Our particular variant of the LD scheme utilizes a discrete variational method (DVM) to solve the Schrödinger equation, using an expansion basis of *numerical* quasiatomic orbitals. In order to minimize the computing effort, a shape approximation is made to the potential (self-consistent-charge approximation, see ref 10) so that the Mulliken atomic orbital populations are the sole parameters of the self-consistent potential. These Mulliken populations, which are determined by the iteration process, help to provide a useful physical interpretation of the resulting charge and spin distributions. Details may be found in previous papers on this method.[9-11]

Free-Base Tetraazaporphyrin

A. Ground-State Energy Levels and Bonding. All calculations were made in square-planar geometry, using average atomic positions from X-ray crystallographic studies,[12,13] as shown in Table I. For reference purposes, the metal-free TAP molecule, $H_2TAP(H_2C_{16}N_8H_8)$, was treated in two geometrical configurations (D_{2h} symmetry): (i) bonded, with H's attached to two opposing nitrogens, and (ii) bridged, with H's shared between adjacent nitrogens. The correct description of the location of the free-base protons has been controversial,[2,3,5] and it is hoped our results will contribute to the resolution of this problem. The

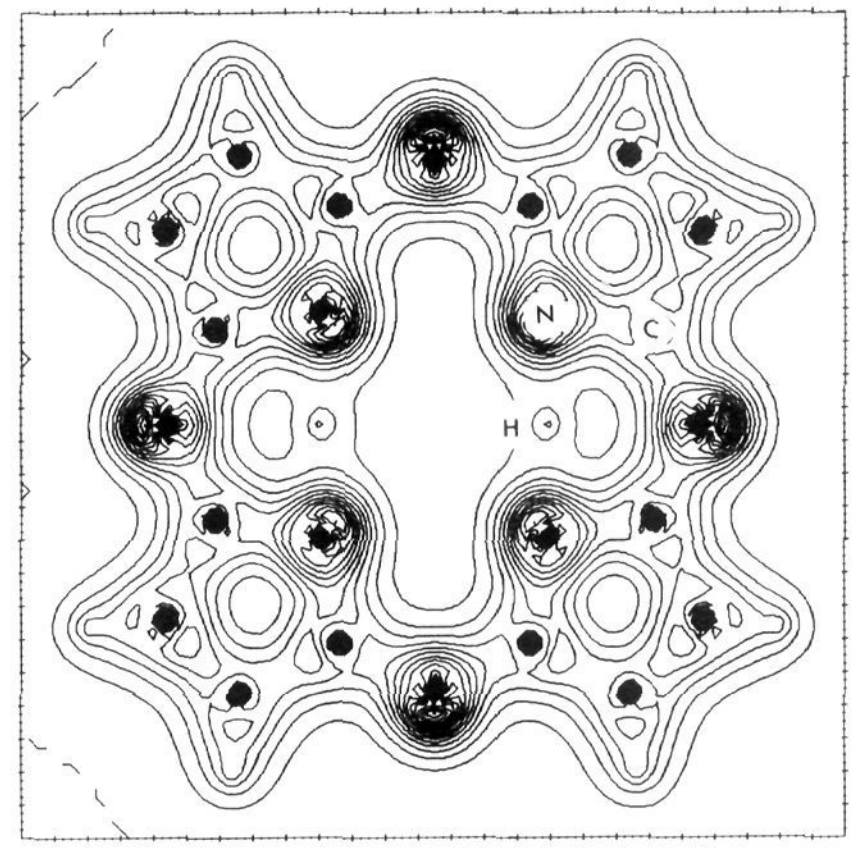

Figure 1. Valence charge density of H_2Pc in the D_{2h} shared configuration. Contour levels are uniformly spaced in the molecular plane at an interval of 0.05 e/a_0^3.

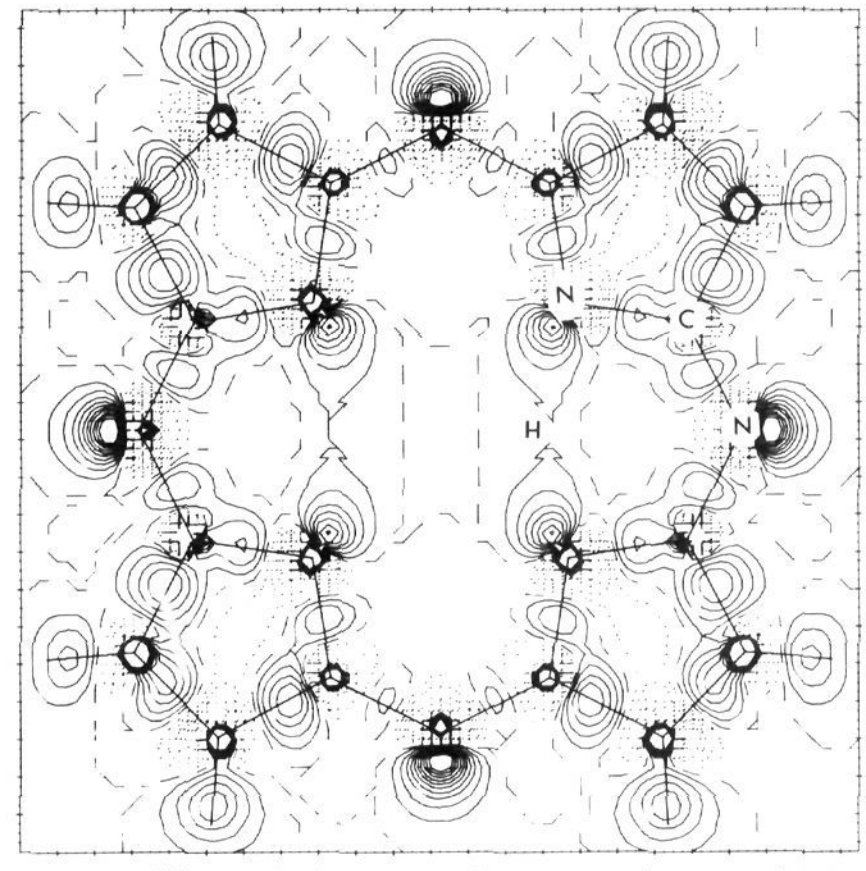

Figure 2. Difference density for shared hydrogen configuration of H_2Pc, in the molecular plane. Regions of negative density are indicated by dotted lines; the zero-density contour is dashed. Contour intervals are 0.1 $e/Å^3$.

(7) G. A. Williams, private communication; G. A. Williams, B. N. Figgis, and R. Mason, *J. Chem. Soc., Dalton Trans.* 734 (1981), analyze neutron data for CoPc; P. Coppens, private communication; X-ray data for MnPc are presented by B. N. Figgis, E. S. Kucharski, and G. A. Williams, *J. Chem. Soc., Dalton Trans.*, 1515 (1980).

(8) J. C. Slater, "Quantum Theory of Molecules and Solids", Vol. 4, McGraw-Hill, New York, 1974.

(9) E. J. Baerends, D. E. Ellis, and P. Ros, *Chem. Phys.*, **2**, 41 (1973).

(10) A. Rosén, D. E. Ellis, H. Adachi, and F. W. Averill, *J. Chem. Phys.*, **65**, 3629 (1976).

(11) D. E. Ellis and Z. Berkovitch-Yellin, *J. Chem. Phys.*, **74**, 2427 (1981).

(12) J. M. Robertson, *J. Chem. Soc.*, 1195 (1936); J. M. Robertson and I. Woodward, *ibid.*, 2 (1937).

(13) For CuPc: C. J. Brown, *J. Chem. Soc. A*, 2488 (1968). For FePc: private communication to B. M. Hoffman from J. L. Hoard. We thank the referee for the additional reference for FePc: J. F. Kirner, W. Dow, and W. R. Scheidt, *Inorg. Chem.*, **15**, 1685 (1976). The Fe–N distance found, 1.927 Å, is in close agreement with the values we have used for FeTAP. For a discussion of bond length variation with metal in MPc, see: W. R. Scheidt and W. Dow, *J. Am. Chem. Soc.*, **99**, 1101 (1977).

Table II. Comparison of Theoretical and Experimental Energy Levels of H_2Pc and H_2TAP (in eV)

experiment[a] (H_2Pc)	PPP-B[b] (H_2Pc)				DVM-B[c] (H_2TAP)				DVM-S[d] (H_2TAP)			
	MO	$-\epsilon$	MO	$-\epsilon$	MO	$-\epsilon$	MO	$-\epsilon$	MO	$-\epsilon$	MO	$-\epsilon$
6.41 s	a_u	5.70	a_g	10.39	b_{1u}	6.9	b_{1u}	12.9	b_{1u}	7.4	b_{2g}	12.2
	b_{1u}	7.18	b_{2u}	10.39	b_{2u}	7.2	b_{2g}	12.9	a_g	7.9	b_{1u}	12.2
8.75 b	b_{2g}	8.18	b_{3u}	10.39	a_g	7.4	b_{2u}	13.2	a_u	8.0	b_{1g}	13.1
	b_{1u}	8.30	a_g	10.39	b_{3g}	7.8	a_g	13.4	b_{2u}	8.1	b_{3u}	13.1
10.24 wp	b_{3g}	8.66	b_{1u}	11.18	b_{1g}	7.8	b_{1g}	13.6	b_{2g}	8.4	b_{2u}	13.5
	b_{2g}	8.85	b_{2g}	11.60	a_u	7.9	b_{3u}	13.7	a_u	8.4	b_{1g}	13.6
11.2 (?) pw	a_u	8.92	b_{1u}	11.77	b_{3u}	8.1	b_{2u}	14.1	b_{3g}	8.4	a_g	13.8
	b_{3g}	9.18	a_u	11.84	b_{2u}	8.4	a_g	14.3	b_{1u}	8.7	b_{2u}	13.8
12.27 pw	b_{1u}	9.23	b_{3g}	11.89	b_{1u}	8.5	b_{1g}	14.3	b_{3u}	8.8	b_{3u}	14.2
12.57 pw	a_u	9.54	b_{1u}	12.62	a_g	8.8	b_{3u}	14.8	b_{1g}	9.0	a_g	14.2
	b_{3g}	10.11	b_{2g}	13.30	b_{2g}	9.5	a_g	15.2	a_g	9.1	b_{1g}	14.7
13.12 dp	b_{2g}	10.22	b_{3g}	13.56	b_{1u}	9.6	b_{3u}	15.2	b_{3g}	9.6	b_{2u}	15.6
	b_{3u}	10.39	b_{1u}	13.81	b_{2g}	9.6	b_{2u}	15.7	b_{2u}	9.7	b_{3u}	15.7
13.92 dp	b_{1g}	10.39			b_{3g}	9.8	a_g	15.8	b_{2g}	9.8	b_{1g}	15.8
					a_u	10.5			b_{1u}	10.6	a_g	16.1
					b_{1u}	11.3			b_{3u}	11.4	b_{3u}	16.1
					b_{3g}	11.4			a_u	11.6	b_{2u}	16.1
					b_{1g}	12.8			b_{3g}	11.9		
					b_{3u}	12.9			a_g	12.1		

[a] Vapor phase photoelectron spectra (ref 6) notation is s = sharp, b = broad peak, wp = weak peak, pw = possible weak peak, dp = distinct peak. [b] Pariser-Parr-Pople "Peel" model (ref 3), in bonded hydrogen configuration. [c] Present calculations, bonded hydrogen configuration. [d] Present calculations, shared hydrogen configuration.

self-consistent ground-state orbital energies for both configurations are compared with photoelectron spectra of H_2Pc and the Pariser–Parr–Pople (PPP) results of Henriksson and Sundbom[3] in Table II. The valence charge density for the bridged configuration is displayed in Figure 1.

Difference density maps, showing contour levels of

$$\Delta\rho = \rho_{\text{molecule}} - \rho_{\text{proto}} \quad (1)$$

are useful in exposing anisotropy and other bonding features of the molecular charge distribution. The choice of the reference prototype ρ_{proto} is partly a matter of taste. We found that either superposition of neutral atomic densities, $\rho_{\text{proto}} = \Sigma_\nu \rho_\nu$, or a superposition of optimized atoms (ions), ρ_{SCC}, consistent with our choice of basis and the self-consistent iteration procedure, give quite similar results. The difference density for the bridged configuration, found from eq 1 by using the ρ_{SCC} density, is given in Figure 2. Here the nitrogen lone pair densities are evident, as is the slight polarization of lone pairs toward the hydrogen sites. The C–N bond charge is noticeably weaker than the C–C component, in accord with X-ray studies of other molecular crystals.[14] The density around protons exterior to the molecular skeleton is rather spherical, somewhat shifted off the nucleus along the C–H axis.

The corresponding $\Delta\rho$ for the bonded configuration, in the molecular plane, is given in Figure 3. Charge density on the ring and hydrogen sites is almost unaffected. The lone pairs associated with H-bonded nitrogen atoms appear to be significantly expanded (delocalized) with respect to unperturbed N densitites. The difference in charge distribution between bridged and bonded configurations is also reflected in one-electron spectra, which we discuss next.

Using a minimal free-atom basis, we find the highest occupied orbital to be $5b_{1u}$ for bonded (B) and bridged (shared = S) configurations with energies of 6.9 and 7.4 eV, respectively, in the ground state. A more precise calculation of the first ionization potential, using Slater's transition-state scheme,[8] increases these values by ~0.5 eV, to be compared with a shoulder on the gas-phase photoelectron spectra (PES) at 6.4 eV. The PPP calculation[3] gives the highest occupied state at 5.7 eV with a_u symmetry. The PES exhibit rather broad bands, with particular features indicated in Table II. There are significant differences among

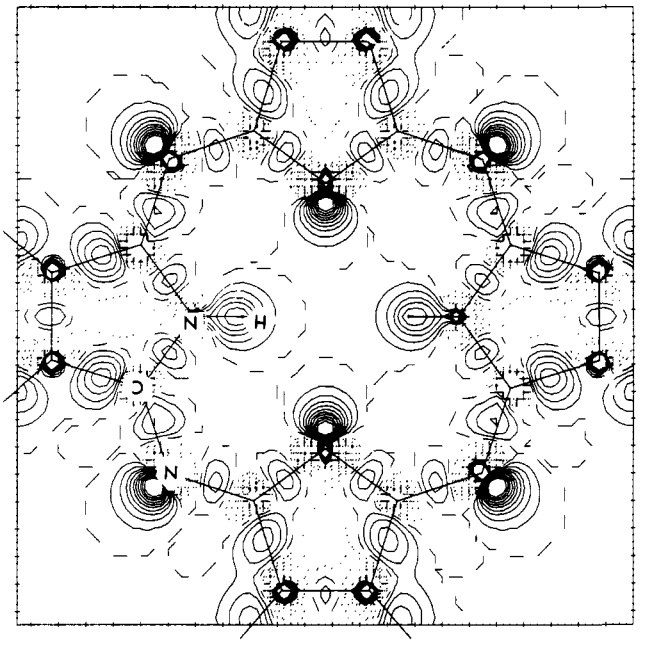

Figure 3. Difference density for bonded hydrogen configuration of H_2Pc, in the molecular plane. Contour intervals are 0.1 e/Å^3.

the level ordering found in the three calculations. For example, we could associate the b_{2g}, b_{1u}, b_{2g}, b_{3g} cluster of levels spanning 9.5–9.8 eV in the bonded configuration with the observed broad peak at 8.8 eV. An alternative explanation based on the b_{3g}, b_{2u}, b_{2g} levels of the shared configuration spanning 9.6–9.8 eV is equally plausible. A critical comparison would require calculation of photo-cross sections to determine line intensities.

B. Optical Spectra. Turning to optical spectra, we present the main features in table III.

The optical transitions calculated for the bonded model by Henriksson and Sundbom,[3] using singly excited configurations (PPP-CI), are in rather good agreement with the vapor-phase spectra.[16] The $a_u \rightarrow b_{3g}$, b_{2g} transitions found by Chen,[5] using the semiempirical Hückel model, are also in reasonable agreement with experiment. In this case the best set of parameter values

(14) P. Coppens and E. D. Stevens, *Adv. Quantum Chem.*, **10**, 1 (1977), and references therein.

(15) G. E. Fichen and R. P. Linstead, *J. Chem. Soc.*, 4846 (1952); J. M. Assour and S. E. Harrison, *J. Am. Chem. Soc.*, **87**, 651 (1965), measurements in solution.

(16) L. Edwards and M. Gouterman, *J. Mol. Spectrosc.*, **33**, 292 (1970); D. Eastwood, L. Edwards, M. Gouterman, and J. Steinfeld, *ibid.*, **20**, 381 (1966).

Table III. Comparison of Theoretical and Experimental Optical Transitions in H_2Pc (in kK)

	expt[a]	PPP-CI-B[b]	DVM-B[c] (H_2TAP)		DVM-S[d] (H_2TAP)	
			$b_{1u} \rightarrow b_{2g}$	7.6	$b_{1u} \rightarrow b_{2g}$	12.6
Q_x	14.6	14.3	b_{3g}	12.7	b_{3g}	14.9
Q_y	16.1	15.9	b_{2g}	34.8	b_{3g}	42.7
			b_{3g}	40.9	b_{2g}	45.3
			$b_{2u} \rightarrow b_{3g}$	14.7	$a_u \rightarrow b_{2g}$	16.8
			b_{3g}	42.9	b_{3g}	19.1
					b_{2g}	46.9
					$b_{2u} \rightarrow b_{3g}$	20.3
B	29.4	26.6	$a_u \rightarrow b_{2g}$	15.5	$a_u \rightarrow b_{2g}$	20.1
			b_{3g}	20.6	b_{3g}	22.4
			b_{2g}	42.7		
			b_{3g}	47.8		
N	35.7	32.2	$b_{3u} \rightarrow b_{2g}$	17.6	$b_{1u} \rightarrow b_{2g}$	23.2
	37.0	32.8	b_{2g}	44.8	b_{3g}	25.5
L	41.7	·	$b_{2u} \rightarrow b_{3g}$	24.7	$b_{2u} \rightarrow b_{3g}$	33.0
		·				
		·				
		·			$b_{1u} \rightarrow b_{2g}$	38.2
C	45.5	(many levels)	$b_{1u} \rightarrow b_{2g}$	20.7	b_{3g}	40.5
		·				
		·				
	47.6	·	b_{3g}	25.8	$a_g \rightarrow b_{1u}$	26.5
		·				
			b_{2g}	47.9		
X_1	55.6		$b_{1u} \rightarrow b_{2g}$	29.3	$b_{2g} \rightarrow b_{1u}$	30.3
			b_{3g}	34.4		49.2
					$b_{3g} \rightarrow b_{1u}$	30.9
X_2	62.5		$a_u \rightarrow b_{2g}$	36.5		
			b_{3g}	41.6		
			$b_{1u} \rightarrow b_{2g}$	43.0		
			$a_g \rightarrow b_{1u}$	38.8	$a_g \rightarrow b_{1u}$	36.6
			$b_{3g} \rightarrow a_u$	25.4	$b_{3g} \rightarrow b_{1u}$	40.0
			b_{1u}	42.0		
			$b_{1g} \rightarrow a_u$	25.4		
			$b_{2g} \rightarrow a_u$	38.9		
			$b_{2g} \rightarrow a_u$	40.0		
			$b_{3g} \rightarrow a_u$	41.6		

[a] Vapor phase absorption spectra, ref 16. [b] Pariser-Parr-Pople singly excited CI model, ref 3, assuming bonded hydrogen configuration. [c] Present calculations, bonded configuration. [d] Present calculations, shared hydrogen configuration.

clearly was found for the shared hydrogen (bridged) configuration. The two theoretical models are, therefore, in conflict with regard to interpretation of the stable molecular configuration. Schaffer and Gouterman used the extended Hückel method with a different set of parameters, and found support for the bonded model.[2]

The present nonempirical results differ from previous studies in assigning b_{1u} as the highest occupied MO. Several other levels intervene, in both bonded and shared models, and the a_u level is found about 1 eV lower. The twofold e(xy,xz) level of D_{4h} symmetry splits into b_{2g}, b_{3g} levels in D_{2h}; this splitting is regarded as the origin of the Q_x, Q_y subbands, with peak separation of ~1.5 kK. On this basis the *shared* model is definitely preferred with $\Delta = (b_{3g} - b_{2g}) = 2.3$ kK, while the *bonded* model predicts $\Delta =$ 5.1 kK. The DVM results given in Table III represent one-electron energy differences, based on *ground* state levels. In order to test the importance of final-state relaxation effects, a transition-state calculation[8] was performed for the $b_{1u} \rightarrow b_{2g}$ (bonded) excitation, increasing the interval from 7.6 to 8.0 kK. This result indicates that relaxation, while significant, is not crucial for describing transitions among diffuse states of rather similar character. Upon examining the dipole-allowed transitions of bonded and shared models, we again definitely prefer the *shared* configuration, with $b_{1u} \rightarrow b_{2g}$, b_{3g} and $a_u \rightarrow b_{2g}$, b_{3g} transitions in reasonable agreement with the Q_x, Q_y bands. The next band of transitions, spanning the region 20–27 kK, is not particularly well-placed relative to the B band centered at 29.4 kK. The spectral features N, L, C can be accounted for by b → b' transitions in the same 30–50 kK energy range. There is obviously considerable room for improving the agreement with experiment, probably indicating that (i) the minimal basis used is inadequate for describing the excited states, (ii) configuration interaction effects may indeed strongly modify the one-electron picture, and (iii) further tests of level sensitivity to the nuclear positions, especially in the shared geometry, would be valuable.

Table IV. Calculated Copper and Iron Tetraazaporphyrin Ground-State Valence Energy Levels (in eV); Spin Polarized DV-SCC-Xα Method Using Iterated Basis

	copper		iron			Cu	Fe
level	spin ↑	spin ↓	spin ↑	spin ↓	level	spin ↑ ≈ ↓	
b_{2u}	3.0[a]	3.0[a]	2.7[a]	2.7[a]	e_u	12.1	11.4
b_{1u}	5.0[a]	5.0[a]	4.6[a]	4.7[a]	b_{1u}	12.4	11.2
e_g	6.4[a]	6.3[a]	6.0[a]	5.5[a]	b_{2u}	12.5	11.8
b_{1g}	7.3	6.9[a]	5.2	3.2[a]	b_{1g}	12.8	12.0 (12.7)[b]
a_{1u}	8.1	8.1	8.0	7.9	a_{2g}	13.0	13.1
e_g	8.7	8.5	8.1	6.6	e_u	13.1	13.1
b_{2u}	8.8	8.7	8.8	8.8	b_{1g}	13.5	13.3
a_{2u}	8.9	8.9	9.1	9.2	e_g	13.6	12.3
a_{2u}	9.4	9.4	8.6	8.6	a_{1g}	13.7	13.0 (13.3)[b]
a_{1g}	9.9	9.4	8.5	6.0[a]	b_{2g}	13.7	13.8
b_{2g}	9.6	9.5	8.6	6.3[a]	e_u	13.8	13.8
e_g	10.2	9.9	9.7	9.1	a_{2u}	14.0	12.5
e_u	10.2	10.2	9.4	9.4	a_{1g}	14.0	13.8
b_{2g}	10.7	10.3	9.5	9.1	a_{2g}	16.1	15.5
a_{1g}	10.7	10.7	9.9	9.9	b_{1g}	16.1	15.9
e_g	11.0	10.9	10.2	10.2	e_u	16.1	16.0
					a_{1g}	16.8	16.6
					a_{2g}	17.0	16.9
					e_u	17.1	16.4
					e_u	17.6	17.4
					b_{2g}	18.0	17.0
					b_{2g}	18.6	18.8
					b_{1g}	19.5	18.5
					e_u	21.0	20.3

[a] Unoccupied level; highest occupied level of either spin is underscored. [b] Spin ↑ value, if different from spin ↓.

Transition-Metal Tetraazaporphyrins

A. Energy Levels and Bonding. The atomic coordinates used for both Cu and Fe tetraazaporphyrin, taken as average values from the X-ray measurements,[13] are given in Table I. Ground-state valence energy levels for the two systems are listed in Table IV for comparison with experiment. It has been remarked that metal-free and transition-metal Pc's exhibit very similar photoelectron spectra,[6] and the calculated levels bear out this observation. Previously, identification of a low-lying PES peak as due to d-electron ionization was made;[6,17,18] however, this has been shown to be an artifact of He^{II} radiation. The PPP calculations of Henriksson et al.[19] on CuPc indicate a highest singly occupied b_{1g} level (D_{4h} symmetry) of strong metallic 3d (x^2-y^2) character (71%). However, the one-electron energy is too low (3.3 eV) compared with the ionization spectra. The present calculations also yield b_{1g} as the last occupied level, with considerable d-electron contribution (52%); now, however the estimated binding energy is in good agreement with experiment. Transition-state calculations produce relaxation-energy shifts of only ~0.5 eV in the valence levels due to their considerable delocalization. This delocalization may be the key to understanding the relatively low-line intensity, compared to free-atom d-electron photo-cross sections. Further calculations of line shape would certainly be desirable.

The valence charge density of CuTAP in the molecular plane is presented in Figure 4. A comparions with the corresponding

(17) J. N. A. Ridyard in "Molecular Spectroscopy-1971", P. Hepple, Ed., Applied Science, Essex, England, 1972, p 96.
(18) M. Gouterman in "The Porphyrins", Vol. 3, D. Dolphin, Ed., Academic, New York, 1978, Chapter IV.
(19) A. Henriksson, B. Roos, and M. Sundbom, *Theor. Chim. Acta*, **27**, 303 (1972), and references therein.

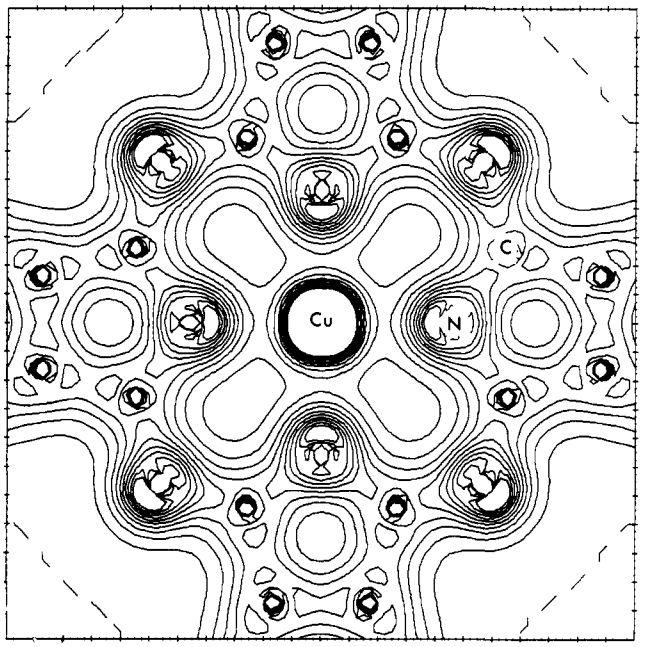

Figure 4. Valence charge density of CuPc, in the molecular plane. Contour levels are spaced at 0.05 e/a_0^3.

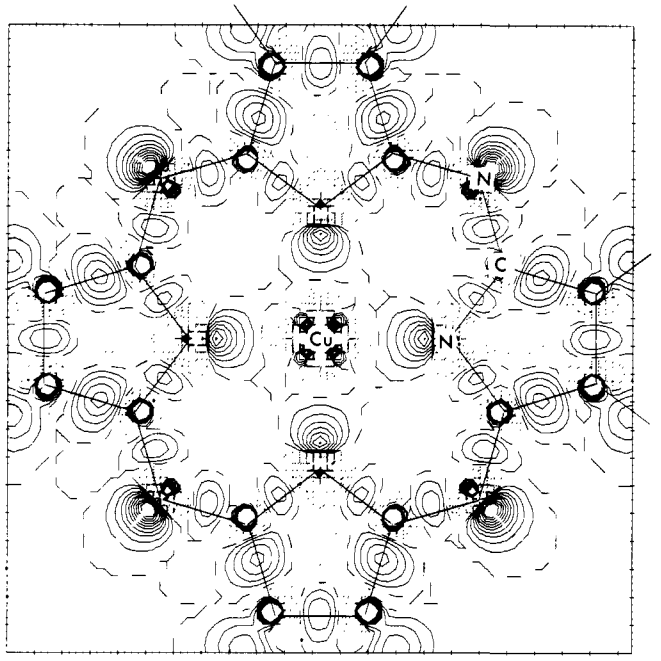

Figure 5. Difference density for CuPc, in the molecular plane. Contour intervals are 0.1 $e/Å^3$.

H_2TAP (shared-H configuration) density of Figure 1 shows the quantitative similarity of density on porphyrin nitrogen sites and indeed on the entire ring structure. In this aspect the copper atom appears as a nearly spherical ion, contributing some density to the interstitial region.

The CuTAP difference density, Figure 5, reveals details of the anisotropic bonding charge. It was formed as $\Delta\rho = \rho(\text{molecule}) - \rho(\text{SCC})$ by subtracting the variationally determined superposition of spherical ions from the molecular density; dotted lines denote negative regions. One can see that charge has been removed from the Cu–N bond region and transferred into fourfold lobes which avoid the "N lone pair" density, which can be interpreted simply as an electrostatic repulsion effect. There is reasonable qualitative agreement between the calculated metal anisotropy and that inferred from X-ray diffraction on MnPc.[7] The anisotropic transfer is superimposed upon the buildup of spherical overlap charge visible in Figure 4.

Table V. Optical Transitions of CuPc and CuTAP (in kK)

	expt[a]	PPP[b] (CuPc)		DVM[d] (CuTAP)	
Q	15.2	^2E_u (S)	18.4	$a_{1u} \rightarrow b_{1g}$	9.6[f]
		^2E_g	20.6[c]	e_g	13.7, 14.5[e]
		^2E_u (S)	34.5	$b_{2u} \rightarrow b_{1g}$	14.5
B	30.8	(S)	35.3	e_g	19.4, 21.8
		$^2B_{2u}$	38.3[c]	$a_{2u} \rightarrow b_{1g}$	16.1[f]
		^2E_u (T)	39.6	e_g	20.2, 21.0
N	36.2 (shoulder)	(T)	39.7	$a_{2u} \rightarrow b_{1g}$	20.2
		(S)	40.1	e_g	24.2, 25.0
		$^2A_{1u}$	41.7	$e_u \rightarrow b_{1g}$	26.6
L	41.6	^2E_u (T)	42.6	$b_{1g} \rightarrow b_{1u}$	18.6[f]
		(S)	42.9	b_{2u}	34.7
		(S)	45.1	$e_g \rightarrow b_{1u}$	28.2, 29.8
C	45.8	$^2A_{2u}$	48.8[c]	b_{2u}	44.4, 46.0
		^2E_u (S)	50.0	$a_{1g} \rightarrow b_{1u}$	35.5, 39.5[f]
				$b_{2g} \rightarrow b_{1u}$	36.3, 37.1
				$e_g \rightarrow b_{1u}$	39.5, 41.9

[a] Center of band, ref 16. [b] Selected states from single-excited semiempirical CI, ref 19. Notation (S) and (T) refer to singdoublet and tripdoublet configuration of porphine ring. [c] Identified as partial charge-transfer transitions; ^2E_g is forbidden. [d] Present calculations; one-electron energy difference using *ground*-state levels. [e] Transitions of spin ↑ and ↓ are given where allowed. [f] Forbidden transition.

Comparison of $\Delta\rho$(CuTAP) with $\Delta\rho(H_2TAP$, shared H) of Figure 2 shows the extent of polarization of bond charges in the latter due to the asymmetric protons. In addition to the N lone pair distortion noted earlier, one sees a significant shift of N–C and C–C bond densities in the D_{2h} molecular field. The bonding charge which can be estimated from contour levels is almost the same in both metal-free and CuTAP. The bond charge deformation is found to be much smaller for the bonded-H configuration of H_2TAP (see Figure 3); the perturbation seems to be essentially localized to the H–N bond.

In Figure 6 we display $\Delta\rho$(CuTAP) on a plane perpendicular to the molecule, containing the Cu–N bond and bisecting the outer C–C bond. The accumulation of density along the z axis on the copper site, due to the $3d_{z^2}$ orbital, is clearly seen, as in the depletion of charge along the Cu–N bond line. The z-direction extension of the N lone pair and the C–C bond are quite similar, while the latter clearly contains much less charge. The C–C bond distribution is seen to have an elliptical cross section, being more extended in the z direction.

B. Optical Spectra. The main band features Q, B, N, L, C found for copper phthalocyanine by Edwards and Gouterman[16] are given in Table V, along with results of semiempirical PPP calculations[19] and the present theory. General features of the spectra strongly resemble those of *metal-free* H_2Pc, and are assigned as $\pi \rightarrow \pi^*$ transitions within the Pc ring (see Table III). The PPP-CI calculations confirm this assignment, with a consistent error of ca. +3 kK in the predicted transition energy. Metal Pc's display additional band features which may be attributed to charge-transfer transitions and $n \rightarrow \pi^*$ excitations modified by metal-ring interactions. A comparison of ZnPc and CuPc spectra[16] shows that the unpaired Cu3d $b_{1g} \rightarrow \pi^*$ (ring) transitions must be buried under the main bands. No new features are visible, but relative intensity of Q and B bands does change and the CuPc Q band is noticeably broader. The PPP results support this view, with partial charge-transfer transition predicted at 20.6, 38.3, and 48.8 kK.

The DVM results given in Table V are simple one-electron energy differences found using *ground*-state levels, uncorrected for relaxation effects, and thus provide only a rough guide to the excitation spectra. The use of an expanded basis and self-consistent determination of relaxation energies could easily change the quoted values by several kilocalories. It is tempting to suppose that the $\pi \rightarrow d$ forbidden transition at 9.6 kK contributes to the low-energy broadening of the Q band. The $a_{1u} \rightarrow e_g$ $\pi \rightarrow \pi^*$ transitions fall in the middle of the Q band, in accordance with the usual assignments. Transitions *into* the half-filled b_{1g} level span the region 10–27 kK, while $d \rightarrow \pi^*$ transitions occur at 19 and 35 kK thus

underlying both Q and Bands. The $a_{2u} \rightarrow e_g\ \pi \rightarrow \pi^*$ transitions believed to dominate the B and N bands are found at too low energy, 20 and 24 kK, respectively, suggesting the importance of final-state relaxation effects. The remaining transitions in the energy range up to 45 kK can be described as $n \rightarrow \pi^*$ ring excitations which contribute to the width of the observed bands, as suggested by Edwards and Gouterman.[16]

Turning now to FeTAP, we see that the $a_{1g}(3z^2-r^2)$ and $b_{2g}(xy)$ hole states ~50% localized on the ferrous ion will lead to a much richer spectrum of additional bands, consistent with experiment. There are at least six additional band features seen in the spectra, and the phthalocyanine window (18–25 kK) is essentially closed.[16] Since rearrangement effects on excitation and multiplet (singlet–triplet) splittings are going to be important, we do not expect quantitative agreement between ground state energy level differences and experiment. The exchange splitting between spin ↑ and ↓ levels becomes as great as 2.5 eV for states of dominant Fe 3d character, and is responsible for the $S = 1$ (actually, $M_S = 1$ is calculated) intermediate spin ground state predicted for FeTAP. This result is consistent with experiment, and not easily obtained in spin-restricted orbital models. For example, Clack and Monshi carried out semiempirical INDO calculations on FePc and attempted to describe the $^3A_{2g}$ ground state as arising from the configuration $e_g^2 b_{2g}^2 a_{1g}^2$ on the basis of total energy arguments. We see that the existence of exchange splittings invalidates the traditional crystal field and ligand field orbital models. The present calculated level ordering and occupation (for predominantly Fe-d MOs) is:

$$\text{spin} \uparrow \qquad b_{2g}^1 \lesssim a_{1g}^1 < e_g^2 \ll b_{1g}^0$$

$$\text{spin} \downarrow \qquad e_g^2 < b_{2g}^0 < a_{1g}^0 \ll b_{1g}^0$$

to give the nominal $(d\uparrow)^4(d\downarrow)^2$ iron d^6 intermediate spin configuration. We agree with these authors that it is necessary to go over to a many-electron framework in order to calculate the low-lying $d \rightarrow d$ transitions with any precision.

From the data in Table IV we can construct a rough picture of expected d–d and d–ring excitations. First, we find the low-energy dipole-forbidden spin-allowed d–d transitions $e_g \rightarrow a_{1g}$, b_{2g} at 4.8 and 7.3 kK; these transitions give a first approximation to the observed bands at 5500, 6400 (weak), and 8200 cm^{-1}.[20] Transitions into the same levels from ring states occur at 21, 23, and 25–30 kK. Transitions *from* the open Fe-3d shell occur at 15 kK ($e_g \rightarrow b_{1u}$) and also contribute in the range 28–44 kK.

C. Spin Density and Hyperfine Fields. In the spin-unrestricted self-consistent-field model used here, the spin density is defined as

$$\rho_s(\vec{r}) = \sum_n f_{n\uparrow}|\psi_{n\uparrow}(\vec{r})|^2 - f_{n\downarrow}|\psi_{n\downarrow}(\vec{r})|^2 \qquad (2)$$

where $f_{n\sigma}$ and $\psi_{n\sigma}$ are occupation numbers and wave functions for spin σ, respectively. In the absence of significant *orbital* contributions to the magnetization density, neutron magnetic scattering data can be inverted by Fourier transformation to generate experimental spin density maps for comparison with ρ_s. This approach may be preferable to comparison of theoretical and experimental form factors when a detailed interpretation of delocalization and covalency effects is desired. Such experimental maps are beginning to be available for the metal phthalocyanines.[7]

In Figure 7 one finds the spin density for CuTAP given in the molecular plane. The result is very simple to understand: (i) The use of Fermi–Dirac statistics in the SCF calculation leads to the unpaired $b_{1g}(Cu3d(x^2-y^2))$ level whose density is visible at the center. (ii) This level is ~50% delocalized onto neighboring N sites, and consequently the unpaired spin is effective at polarizing the N atoms. A node in the density along the Cu–N bond line is noted. (iii) More distant atoms are weakly polarized by the exchange interaction with the unpaired spin. Further aspects of the CuPc magnetization are discussed below in connection with hyperfine fields.

(20) D. W. Clack and M. Menshi, *Inor. Chim. Acta*, **22**, 261 (1977), and references therein.

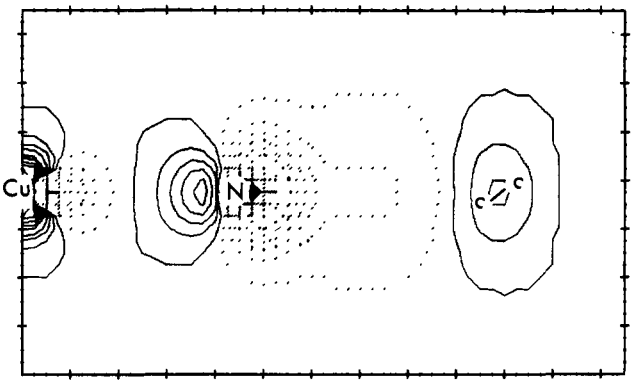

Figure 6. Difference density for CuPc, in the plane perpendicular to the molecule through the C–N bond, bisecting the C–C bond. Contour intervals are 0.1 e/Å^3.

In the case of iron tetraazaporphyrin, the self-consistent ground state is found to have two unpaired levels, $b_{2g}(xy)$ and $a_{1g}(3z^2-r^2)$ corresponding to a predicted intermediate spin. In contrast to CuTAP, we now find (see Figure 8, note use of a log scale) that the N lone pair is *negatively* polarized. In fact the porphyrin N-atom polarization is seen to be rather complex, with positive lobes connecting to outer ring C–N–C groups. These results have been briefly reported elsewhere.[21]

Electron spin resonance and ENDOR spectroscopy have been extensively used to probe hyperfine fields in the vicinity of metal ions, nitrogen ligands, and proton sites for a variety of metalloporphyrins.[22,23] Parametrized molecular orbital models have been fitted to the isotropic (contact) and spin-dipolar magnetic hyperfine Hamiltonian to determine covalency and crystal field splitting parameters. In some cases the electric field gradient is also determined from the nuclear electric quadrupole interaction,[23] providing additional parameters to describe the electronic charge distribution. In certain cases (e.g., iron, tin, and ruthenium compounds) Mössbauer γ resonance spectroscopy can provide precise data on both magnetic and electric hyperfine fields. Such measurements have been made on FePc.[24,25]

We have shown, in previous work on Cu and Ag porphine,[11] that the simple semiempirical models omit important contributions to hyperfine fields arising from polarization of closed shell orbitals. These contributions are of course averaged into effective single orbital $\langle r^{-3} \rangle$ matrix elements and covalency parameters, and then efforts made to interpret systematic changes with metal ion or ring substitutions. One goal of our calculations is to separately determine fields due to unpaired electrons and the response of the doubly occupied orbitals, in order to rationalize experimental trends. The measured magnetic hyperfine tensor components $A_\parallel$ and $A_\perp$ contain a superposition of spin and orbital moment terms, which show variations of ~10% across the series CuX, X = P, TPP, Pc, TPy, TBP, etc.[22] The spin dipolar matrix elements $d_z(i) = \langle i|(3z^2-r^2)/r^5|i\rangle$ for the unpaired $10b_{1g}$ level in Cu porphine and TAP are −2.98 and $-3.08a_0^{-3}$, respectively. However, contributions form the first 11 doubly occupied levels change the net interaction $D_z = \sum_i^{occ} 2s_{z,i}\, d_z(i)$ to −3.50 and $-2.87a_0^{-3}$, respectively.[26] Thus the polarization response of CuP is seen to be antishielding (adds to unpaired spin) while that of CuTAP is

(21) D. E. Ellis and Z. Berkovitch-Yellin, Proceedings of the Conference on Magnetism and Magnetic Materials, Dallas, Oct 1980; *J. Appl. Phys.*, to be published.

(22) P. W. Lau and W. C. Lin, *J. Inorg. Nucl. Chem.*, **37**, 2389 (1975); C. M. Guzy, J. B. Raynor, and M. C. R. Symons, *J. Chem. Soc. A*, 2299 (1969).

(23) T. G. Brown and B. M. Hoffman, *Mol. Phys.*, **39**, 1073 (1980), and references therein.

(24) I. Dézsi, A. Balázs, B. Molnár, V. D. Gorobchenko, and I. I. Lukashevich, *J. Inorg. Nucl. Chem.*, **31**, 1661 (1969).

(25) A. Hudson and H. J. Whitfield, *Inorg. Chem.*, **6**, 1120 (1)967).

(26) The spin dipolar energy can be conveniently written as $\vec{H}_{sd} = g_N\beta_N\vec{I}_N \cdot \vec{H}_{sd}$ where $\vec{I}_N$ is the nuclear spin and the effective field is $\vec{H}_{sd} = g_e\beta_e\langle\psi|(3(\vec{r}\cdot\vec{s})\vec{r} - r^2\vec{s})/r^5|\psi\rangle$. The conversion factor to magnetic field from atomic units is conveniently given as $\beta_e = e\hbar/2mc = (62.6\ kG)a_0^3$.

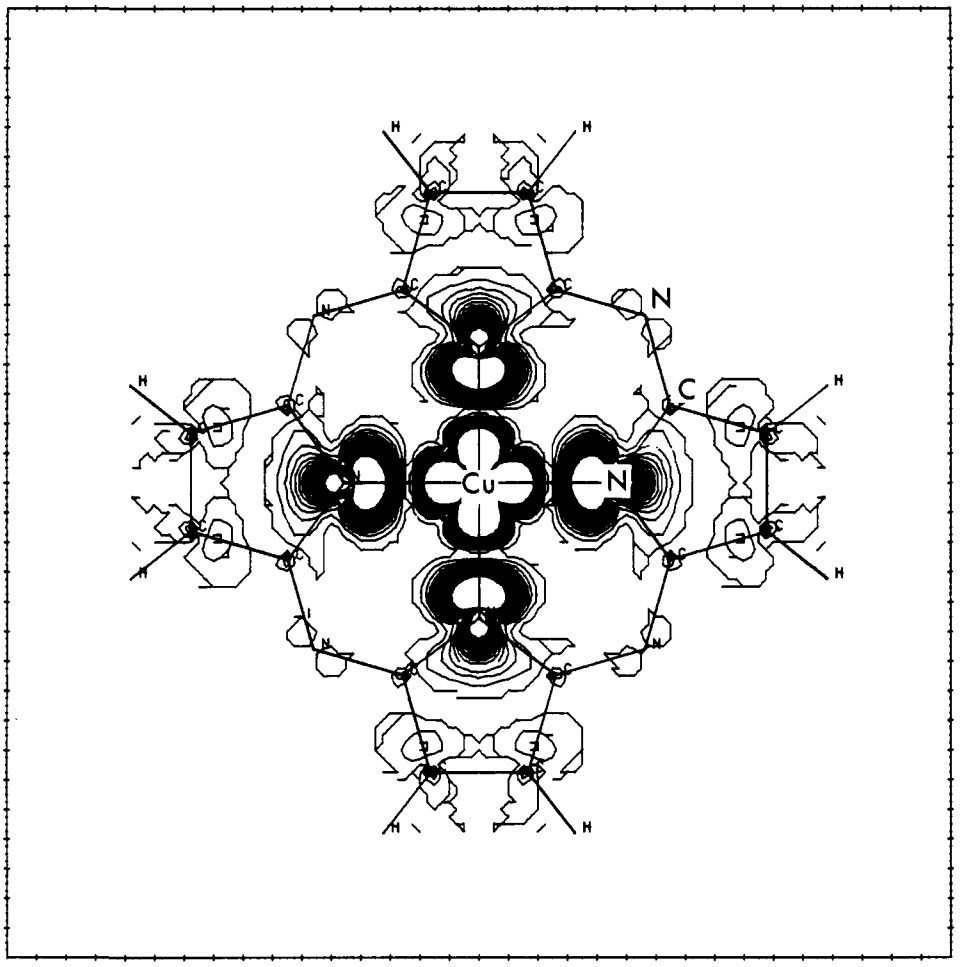

Figure 7. Spin density for CuPc in the molecule plane. Contour intervals are 0.0004 e/Å^3.

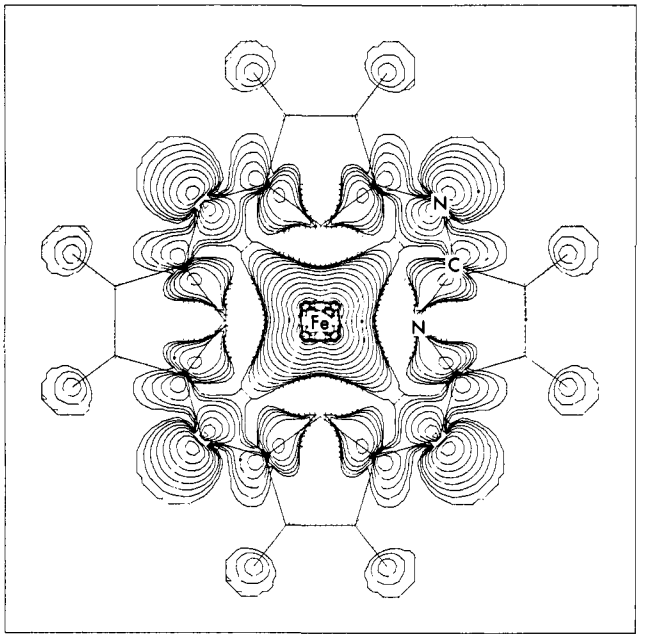

Figure 8. Spin density for FePc in the molecular plane. Logarithmic contour levels are ±5, ±10, ±20, ...x× 10^{-6} e/Å^3.

weaker, and shielding in character. It will be necessary to sum over essentially the entire valence band, and to explore the numerical stability of such results (variation with basis sets, shape approximation in potential, etc.) before making serious numerical comparisons with experiment. The present results would predict an ~18% change in spin dipolar contributions to both $A_\parallel$ and $A_\perp$, but we must expect equally significant changes in the contact field due to spin density at the nucleus, $\rho_s(0)$. The calculated value $\rho_s \approx 0$ at the Cu nucleus for either compound is unfortunately not accurate, due to our use of spin-restricted atomic functions as the molecular variational basis. Thus essential core-level polarization is not adequately treated.

The transferred hyperfine field at the porphyrin nitrogen site has been calculated for CuP and CuTAP. The $10b_{1g}$ contribution is $-0.13a_0^{-3}$ for both molecules, reduced to –0.06 (CuP) and –0.10 (CuTAP) by screening contributions of doubly filled orbitals. Since the screening is of the same magnitude as the net interaction, it is clear that single orbital models are inadequate. For the next-nearest neighbor carbon site in CuTAP, we find the net value $D = +0.009a_0^{-3}$ compared to the "direct" contribution $d(10b_{1g}) = -0.003$. The sign of this interaction is *not* known experimentally, and it appears that two- and three-center off-site terms dominate. Similarly, values for the bridge nitrogen site are found to be $D = +0.011$, $d(10b_{1g}) = -0.003a_0^{-3}$.

Spin resonance data for FePc do not seem to be available, but several Mössbauer studies have been made.[24,25] The magnetic moment of 3.83 μ_B[27] and the isomer shift value $\delta = 0.6$ mm/s are intermediate to high-spin ($S = 2$) and low-spin ($S = 1$) values. On the basis of spin-restricted Hückel calculations for iron porphine[28] Dézsi et al.[24] propose the configuration $(b_{2g})^2(e_g)^3(a_{1g})^1(b_{1g})^1$ with three unpaired spin and $S = {}^3/_2$. This assignment conflicts with the $^3A_{2g}$ ground state determined by other workers.[20] As can be seen from the data from Table IV, exchange splittings of ~2.5 eV separate spin ↑ from spin ↓ levels in those states with dominant Fe 3d character, considerably modifying the single particle energy level scheme. We find a "Fe 3d Level" ordering $b_{2g} < a_{1g} < e_g < b_{1g}^* < a_{1g}^* < e_g^* < b_{2g}^*$ for majority spin and $e_g < b_{2g}^* < a_{1g}^* <$

(27) A. B. P. Lever, *J. Chem. Soc.*, 1821 (1965).
(28) M. Zerner, M. Gouterman, and H. Kobayashi, *Theor. Chim. Acta*, **6**, 363 (1966).

b_{1g}* for minority spin. The net result is spin unpairing of b_{2g} and a_{1g} levels. Mulliken population analysis yields the configuration $Fe^{+1.68}$ 3d(6.09) 4s(0.09) 4p(0.18) with 2.53 unpaired 3d electrons. The calculated contact field is H_c = 330 kG.

In principle one can calculate the electric field gradient for comparison with the measured quadrupole splitting ΔE = 2.6 mm/s.[24] In practice we have found so many large and cancelling contributions across the entire valence band (not to mention core polarization!) that at present there is insufficient numerical precision to make a significant test of this parameter. We are making efforts to correct this deficiency.

Conclusions

Ground state energy levels and charge and spin densities have been calculated for H_2TAP, CuTAP, and FeTAP, using the nonempirical Hartree–Fock–Slater model. The energy levels correlate well with photoelectron binding energies, and it is hoped that X-ray and neutron diffraction data will shortly be available to verify the densities. The local density theory is on less firm ground in treating excitations; however, the simple estimates of optical transitions prove to be useful in validating semiempirical model interpretations. With regard to magnetic and electric hyperfine fields, we find that the simplest MO models used in fitting spin resonance and Mössbauer data omit important polarization (screening) effects which extend across the valence band. With the present computational approach these effects can be crudely mapped, but further development is needed in order to make quantitative hyperfine parameter predictions.

Acknowledgment. Partial support by the National Science Foundation (Grant No. CHE-7812234) and a grant of computer time from the National Resource for Computation in Chemistry is acknowledged. One of us (Z.B.-Y) gratefully acknowledges support through a Chaim Weizmann Fellowship. D.E.E. acknowledges support by the NSF-MRL program through the Materials Research Center of Northwestern University (Grant No. DMR79-23573). We wish to thank Mark Ratner and Joseph Berkowitz for suggestions and encouragement.

Static and Dynamic Stereochemistry of Hexaethylbenzene and of Its Tricarbonylchromium, Tricarbonylmolybdenum, and Dicarbonyl(triphenylphosphine)chromium Complexes

Daniel J. Iverson,[1a] Goeffrey Hunter,[1a,b] John F. Blount,[1c] James R. Damewood, Jr.,[1a] and Kurt Mislow*[1a]

Contribution from the Department of Chemistry, Princeton University, Princeton, New Jersey 08544, and the Chemical Research Department, Hoffmann-La Roche, Inc., Nutley, New Jersey 07110. *Received February 17, 1981*

Abstract: The crystal and molecular structures of hexaethylbenzene (**1**), tricarbonyl(hexaethylbenzene)chromium(0) (**2**), tricarbonyl(hexaethylbenzene)molybdenum(0) (**3**), and dicarbonyl(hexaethylbenzene)(triphenylphosphine)chromium(0) (**4**) have been determined. Crystallographic data for **1–4** are collected in Table VI. The methyl groups in **1–3** project alternately above and below the least-squares plane of the benzene ring. In **2** and **3**, three of the ethyl groups are eclipsed by the carbonyl groups; the corresponding methyl groups project toward the uncomplexed side of the ring. The barrier to site exchange (ΔG^*) of the ethyl groups in **2** and **3** is ca. 11.5 kcal mol^{-1}, as determined by dynamic NMR spectroscopy. This value is to be compared with the ethyl rotation barrier of 11.8 kcal mol^{-1} estimated for **1** by empirical force field calculations. According to these calculations, the ground-state structure of **1** (D_{3d}) is substantially the same as the conformation in the crystal, and the ethyl group rotations are not correlated (concerted). The structure of **4** differs markedly from those of **1–3**, in that all six methyl groups now project toward the uncomplexed side of the ring, and the molecule assumes a staggered rather than an eclipsed conformation (see Figure 6). Several features of the X-ray structure indicate that this conformational change may be ascribed to steric effects of the triphenylphosphine group.

This report deals with stereochemical features of systems in which hexaethylbenzene functions as the η^6-arene in tricarbonylchromium and related transition-metal complexes.[2,3] Hexaethylbenzene is a representative of a class of hexaalkylbenzenes or hexaalkylbenzene analogues in which the alkyl groups are observed or predicted to point alternately up and down around the ring perimeter, so as to impart approximate D_{3d} or S_6 symmetry to the molecule. The parent compound in this class, hexamethylbenzene, has D_{3d} symmetry;[4] other examples are hexakis(bromomethyl)benzene,[5] hexacyclopropylbenzene,[6] MacNicol's "hexa-host" compounds,[7] hexakis(trimethylsilylmethyl)benzene,[8] and the as yet unknown hexaneopentylbenzene.[9,10] The center

(1) (a) Princeton University. (b) On leave from the Department of Chemistry, University of Dundee, Scotland. (c) Hoffmann-La Roche, Inc.

(2) For comprehensive reviews and leading references to the chemistry of tricarbonyl(η^6-arene)transition-metal complexes (M = Cr, Mo, W), see: Sneeden, R. P. E. "Organochromium Compounds"; Academic Press: New York, 1975; p 19 ff. Silverthorn, W. E. In Stone, F. G. A.; West, R., Eds. "Advances in Organometallic Chemistry"; Academic Press: New York, 1975; Vol. 13, p 48 ff. For a recent update on the literature, see: Atwood, J. D. *J. Organomet. Chem.* **1980**, *196*, 79.

(3) A portion of this work was reported in a preliminary communication: Hunter, G.; Iverson, D. J.; Mislow, K.; Blount, J. F. *J. Am. Chem. Soc.* **1980**, *102*, 5942.

(4) Iroff, L. D. *J. Comput. Chem.* **1980**, *1*, 76 and references therein.

(5) Marsau, M. P. *Acta Crystallogr.* **1965**, *18*, 851.

(6) Bar, I.; Bernstein, J.; Christensen, A. *Tetrahedron* **1977**, *33*, 3177.

(7) MacNicol, D. D.; Hardy, A. D. U.; Wilson, D. R. *Nature (London)* **1977**, *266*, 611. MacNicol, D. D.; McKendrick, J. J.; Wilson, D. R. *Chem. Soc. Rev.* **1978**, 65. Hardy, A. D. U.; MacNicol, D. D.; Swanson, S.; Wilson, D. R. *Tetrahedron Lett.* **1978**, 3579. Hardy, A. D. U.; MacNicol, D. D.; Wilson, D. R. *J. Chem. Soc., Perkin Trans. 2* **1979**, 1011. Hardy, A. D. U.; MacNicol, D. D.; Swanson, S.; Wilson, D. R. *Ibid.* **1980**, 999. Freer, A.; Gilmore, C. J.; MacNicol, D. D.; Wilson, D. R. *Tetrahedron Lett.* **1980**, *1159*.

(8) Bock, H.; Kaim, W. *Chem. Ber.* **1978**, *111*, 3552.

(9) Tidwell, T. T. *Tetrahedron* **1978**, *34*, 1855.

0002-7863/81/1503-6073$01.25/0